Optics Letters

General framework for the analysis of imperfections in nonlinear systems

Matteo Santandrea,* Michael Stefszky, and Christine Silberhorn

Integrated Quantum Optics, Paderborn University, Warburger Straße 100, 33098 Paderborn, Germany
**Corresponding author: matteo.santandrea@upb.de*

Received 25 June 2019; revised 4 October 2019; accepted 4 October 2019; posted 7 October 2019 (Doc. ID 370932); published 4 November 2019

In this Letter, we derive a framework to understand the effect of imperfections on the phase-matching spectrum of a wide class of nonlinear systems. We show that this framework is applicable to many physical systems, such as waveguides or fibers. Furthermore, this treatment reveals that the product of the system length and magnitude of the imperfections completely determines the phase-matching properties of these systems, thus offering a general rule for system design. Additionally, our framework provides a simple method to compare the performance of a wide range of nonlinear systems.

https://doi.org/10.1364/OL.44.005398

In both classical and in quantum optics, nonlinear phase-matching processes are fundamental tools for the generation, manipulation, and detection of a plethora of different states of light, e.g., frequency doubling [1], pulse spectra characterization [2,3], parametric downconversion for photon pair generation [4], frequency upconversion for enhanced single photon detection [5], and frequency conversion for interfacing different quantum memories [6]. These processes are usually realized in $\chi^{(2)}$ or $\chi^{(3)}$ nonlinear systems, e.g., lithium niobate crystals (bulk or waveguides) or photonic crystal fibers (PCFs).

The fabrication of such systems, despite being very mature in many cases, is still affected by imperfections that spoil the phase-matching spectrum of the process. This spectrum is the critical parameter in the case of many quantum systems, as exemplified by the quantum pulse gate [7]; furthermore, the quality of the spectrum is directly related to the efficiency [8]. Therefore, in the past decades, several studies have discussed the relation between fabrication errors in waveguides [8–15] and in fibers [16–19] and their spectral performance.

These previous investigations typically considered only specific types of imperfections. This includes our previous work [8], in which the analysis was restricted to fabrication imperfections affecting the widths of lithium niobate waveguides. Comparing these studies, one can note that the analyzed systems exhibit a close connection between the device length, the amount of imperfections, and the overall performance of the nonlinear process. This observation suggests the existence of a scaling law, common to all nonlinear systems, determining the length where the process becomes sensitive to the imperfections present in the system.

In this Letter, we introduce a general framework for the analysis of imperfections in nonlinear systems, which is system-independent and, thus, allows a systematic comparison of different material platforms. We show that this widely encompassing framework provides important rules to predict and design the behavior of many nonlinear systems.

Consider a nonlinear process in a system of length L characterized by a momentum mismatch:

$$\Delta\beta = \sum_i s_i\beta_i = \sum_i s_i \frac{2\pi n_i(\lambda_i)}{\lambda_i}, \tag{1}$$

where β_i, n_i, and λ_i are the propagation constant, the refractive index, and the wavelength of the ith field, respectively; and $s_i = \pm 1$ is a sign that depends on the type of process considered, for example, for copropagating three-wave-mixing $\Delta\beta = \beta_3 - \beta_2 - \beta_1$. Note that Eq. (1) is valid for any general wave-mixing process. The phase-matching spectrum of the nonlinear process, normalized per unit length, is defined as [10]

$$\Phi = \frac{1}{L}\int_0^L \exp\left\{ i \int_0^z \Delta\beta(\xi)\mathrm{d}\xi \right\}\mathrm{d}z, \tag{2}$$

where z denotes the propagation axis along the system and scaling constants have been neglected, since they do not affect the shape of the phase-matching spectrum. Note that Eq. (2) sets the ideal maximum efficiency is 1. Typically, the phase-matching Φ is expressed as a function of the wavelengths or the frequencies of the fields involved in the process. However, this prevents a direct comparison of different systems, since $\Delta\beta$ depends nonlinearly on these parameters, as shown in Eq. (1). Therefore, in the rest of the Letter, we will consider the phase matching as a function of the $\Delta\beta$.

Under ideal fabrication and operation conditions, the momentum mismatch $\Delta\beta$ is constant along the sample. However, fabrication imperfections and/or non-ideal operating conditions affect the phase mismatch of the process, and they can be described as a position-dependent $\Delta\beta(z)$. If the variation of the momentum mismatch is sufficiently small such that it can be considered frequency-independent [20], we can introduce the *decoupling approximation*

$$\Delta\beta(z) \approx \Delta\beta_0 + \sigma\delta\beta(z), \tag{3}$$

where the momentum mismatch has been decomposed into the sum of $\Delta\beta_0$, describing the momentum mismatch of the process in the absence of inhomogeneities, and $\sigma\delta\beta(z)$, which encompasses the variation of $\Delta\beta$ due to inhomogeneities in the system. The noise amplitude σ is chosen such that $|\delta\beta(z)| \leq 1$.

Under these assumptions and with a change of variables $z/L \to z'$ and $\xi/L \to \xi'$, the integral in (2) can be rewritten as

$$\Phi(\Delta\beta_0 L) = \int_0^1 \exp\{i\Delta\beta_0 L z'\} \times \exp\left\{i\sigma L \int_0^{z'} \delta\beta(L\xi')\mathrm{d}\xi'\right\}\mathrm{d}z', \tag{4}$$

where the first exponential term leads to the usual sinc dependence of the phase-matching Φ on the mismatch $\Delta\beta_0$, while the second exponential term describes the effect of the noise $\sigma\delta\beta(z)$ on the system. Equation (4) can also be understood as the Fourier transform of the rectangular function representing the crystal, multiplied by a phase factor introduced by the imperfections.

In particular, the first exponential shows that the phase-matching spectrum of all noiseless systems is identical, bar a scaling factor given by the length of the system. The second exponential highlights that all systems with the same *noise-length product* σL and noise profile $\delta\beta(z)$, defined for $z \in [0, L]$, will exhibit the same phase-matching spectrum. This allows us to study the effect of variations of the momentum mismatch on a system with unit length and then extrapolate the results to systems with any length, provided the correct scaling $\Delta\beta_0 \to \Delta\beta_0 L$ and $\sigma \to \sigma L$ is applied.

In the previous section, it was shown that the phase-matching spectrum $\Phi(\Delta\beta_0)$ is fully characterized by the noise-length product σL and the noise profile $\delta\beta(z)$. Therefore, in the following, we study the impact of these two parameters on the profile of the phase-matching spectrum.

The scaling law presented in the previous section allows us to consider a general nonlinear system with $L = 1$ m and $\sigma \in [0.001, 1000]$ m^{-1} without loss of generality. We model $\delta\beta(z)$ as a stochastic process with a $1/f$ spectral density to describe the long-range correlations that can arise due to fabrication imperfections and/or under non-ideal operating conditions of the nonlinear system [8]. For each value of σL, we randomly generate 100 different $\delta\beta(z)$ profiles and calculate the relative phase matching as a function of $\Delta\beta_0$ using a piecewise approximation [18] of Eq. (4):

$$\Phi(\Delta\beta_0) = \sum_{n=1}^{N} \mathrm{sinc}\left(\frac{\Delta\beta_n \Delta z_n}{2}\right) \exp\left\{i\frac{\Delta\beta_n \Delta z_n}{2}\right\} \times \exp\left\{i\sum_{m=1}^{n-1} \Delta\beta_m \Delta z_m\right\}, \tag{5}$$

where Δz is the mesh discretization along the z axis, such that $\sum_n \Delta z_n = L$, and $\Delta\beta_n = \Delta\beta_0 + \delta\beta(z_n)$. The simulations presented in this Letter have been performed with the Python package *PyNumericalPhasematching* v1.0b [21].

To quantify the difference between the phase-matching Φ_{noisy} of a system with imperfections and the phase-matching Φ_{ideal} of an ideal one, i.e., where $\delta\beta(z) = 0$, we introduce the fidelity $\mathcal{F}$, defined as

$$\mathcal{F} = \frac{\max_\tau \int_{-\infty}^{+\infty} I_{\mathrm{ideal}}(\Delta\beta_0) I_{\mathrm{noisy}}(\Delta\beta_0 - \tau)\mathrm{d}\Delta\beta_0}{\int_{-\infty}^{+\infty} I_{\mathrm{ideal}}^2(\Delta\beta_0)\mathrm{d}\Delta\beta_0}, \tag{6}$$

where $I = |\Phi|^2$. In Eq. (6), the two curves are normalized such that $\int |\Phi_{\mathrm{noisy}}|^2 \mathrm{d}\Delta\beta = \int |\Phi_{\mathrm{ideal}}|^2 \mathrm{d}\Delta\beta$, since this quantity is conserved in the presence of momentum mismatch variation [22]. Using this definition, the fidelity approaches 1 if the effect of noise on the phase-matching spectrum is negligible and tends to 0 if the contribution of the noise is dominant.

We calculate the fidelity $\mathcal{F}$ for the simulated phase-matching spectra, and the results are plotted in Fig. 1. The results can be well approximated by a Lorentzian-like fitting curve, shown in Fig. 1 with a solid orange line:

$$\mathcal{F}(\sigma L) = \frac{1}{[1 + A \cdot (\sigma L)^B]^C}, \tag{7}$$

with $A = 5.4(3) \times 10^{-3}$, $B = 2.12(4)$, $C = 0.35(2)$.

The simulations show that systems with $\sigma L \leq 10$ have a fidelity close to 1 while, for $\sigma L > 10$, the average fidelity rapidly drops below 0.5. Therefore, the condition $\sigma L \leq 10$ represents a general design principle for these systems.

We now move away from the abstract description, in terms of $\delta\beta$, to study how fabrication imperfections directly relate to the phase matching and to show how the condition $\sigma L \leq 10$ aids in designing a given nonlinear process. For simplicity, we assume that all the imperfections are introduced by a single system parameter f. For example, f could represent the local temperature of the system during operations, the width of a waveguide, or the holes' diameter in a PCF. With a suitable model of the system, one can relate the noise amplitude σ to the variation of the parameter f with a Taylor expansion $\sigma \approx |\partial_f \Delta\beta| \delta f$. Therefore, the condition $\sigma L \leq 10$ can be rewritten as

$$\sigma L \leq 10 \Rightarrow \delta f \cdot L \leq \frac{10}{|\partial_f \Delta\beta|}. \tag{8}$$

In this form, the trade-off between the physical parameters characterizing the sample, namely, its length L and the error δf, is explicitly revealed.

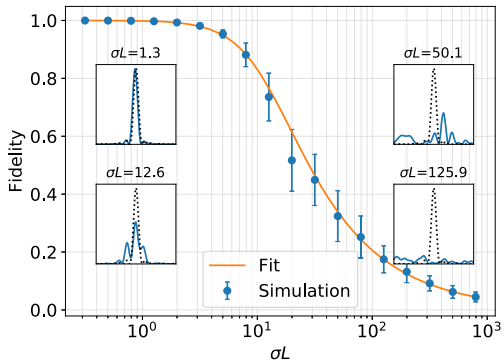

Fig. 1. Simulated reduction in fidelity $\mathcal{F}$ as the noise-length product σL of a nonlinear system increases. The error bars indicate the standard deviations calculated from 100 randomly generated samples. The solid orange line corresponds to the best fit of the average fidelity and follows the relation given by Eq. (7). The insets show examples of simulated phase-matching spectra (solid blue line), compared to the ideal phase-matching spectra (dotted black line), for chosen σL values.

If $|\partial_f \Delta\beta|$ is known, with the help of Eq. (8), one can bound the maximum length of the system to the maximum error during fabrication/operation in order to ensure high fidelity. This can provide crucial information during the design of samples and experiments: if the error δf cannot be further reduced, then the maximum length of the system to achieve high fidelity is bounded by (8); vice versa, if the length of the sample is constrained by the experiment, then the error δf has to be minimized to satisfy (8).

As an example, we consider the restraints set by Eq. (8) on the four-wave-mixing, seeded parametric downconversion process in a PCF described in Ref. [18]. In the Letter, the authors show that a 3 m long fiber presents a very distorted phase matching, while a 15 cm long piece of the same fiber is characterized by a much cleaner, but still imperfect spectrum. In particular, they investigate the effects of the variation of the pitch Λ of the holes and their diameter d around the ideal design parameters $\Lambda_0 = 1.49$ μm and $d = 0.6414$ μm. Using the Sellmeier equations provided in Ref. [23], we can estimate the effect of the variation of these parameters by calculating the partial derivatives:

$$|\partial_\Lambda \Delta\beta|_{\Lambda_0, d_0} \approx 2 \times 10^{-4}\ \mu\text{m}^{-2},$$
$$|\partial_d \Delta\beta|_{\Lambda_0, d_0} \approx 1.5 \times 10^{-2}\ \mu\text{m}^{-2}. \quad (9)$$

Since $\partial_d \Delta\beta$ is two orders of magnitude higher than $\partial_\Lambda \Delta\beta$, the resulting phase matching is much more sensitive to variations of the holes' diameter d than to variations in the pitch.

From the observation that the reported phase matching is already degraded for a PCF longer than 30 cm (which implies that $\sigma L \geq 10$), we can infer that the original 3 m long PCF had a $\sigma L \geq 100$. Using Eq. (7), the expected fidelity for this noise-length product is below 0.2, thereby explaining the distorted phase-matching spectrum measured in Ref. [18]. Finally, combining (8) and (9), we can estimate that it is necessary to limit $\delta\Lambda$ (δd) below 1.1% (0.078%) to achieve high-fidelity phase matching in a 3 m long fiber, clearly a challenging task.

The *decoupling approximation* introduced in Eq. (3) relies on the assumption that the refractive index variation due to imperfections can be considered independent of the wavelength [20]. To show that this approximation is indeed valid in many cases of interest, we now compare the results presented in Fig. 1 with simulations of five different processes in various systems affected by different sources of imperfections, all presenting a $1/f$ noise spectrum.

Process (a) is a type-0 ($zz \to z$) second-harmonic generation (SHG) pumped at 1550 nm in Z-cut, X-propagating titanium indiffused lithium niobate (Ti:LN) channel waveguides. Before indiffusion, the Ti stripe thickness is 80 nm, and its nominal width is 7 μm. We consider fabrication errors on the Ti stripe widths with a maximum excursion of δw. The Ti indiffusion is performed at 1060°C for 8.5 h. The operation temperature of the system is considered to be fixed at 190°C. The model used to calculate the waveguide dispersion is described in Ref. [24].

Process (b) is a type-II ($yz \to y$) SHG pumped at 1550 nm in Z-cut, X-propagating rubidium exchanged potassium titanyl phosphate (Rb:KTP) channel waveguides. We assume waveguide widths of 3 μm, waveguide depths of 8 μm, and a fabrication error on the waveguide width with a maximum excursion of δw. The dispersion of the waveguide is modelled according to Ref. [25].

Process (c) is a type-II ($yz \to y$) sum frequency generation (SFG) 1550 nm + 875 nm → 559 nm in a Z-cut, X-propagating bulk LN crystal. We assume a position-dependent temperature profile of the crystal around the nominal temperature of 190°C. The temperature variation has a maximum excursion of δT. The temperature dependence of the refractive index has been modelled using the Sellmeier equations reported in Ref. [26].

Process (d) is a SFG 1545 nm + 805 nm → 1058.5 nm in a PCF [18]. The nominal pitch of the fiber is $\Lambda = 1.49$ μm, and the holes' diameter is 641.4 nm with a noise that has a maximum excursion of δd. We simulate the dispersion of the system using the model in Ref. [23].

Process (e) is a type-II ($xz \to x$) SHG pumped at 1550 nm in X-cut lithium niobate-on-insulator (LNOI) waveguides. The waveguide has a trapezoidal cross section [27]: its height is 450 nm and coincides with the LN thin film thickness, while its width is 0.9 μm, measured at the top of the profile, and is characterized by a noise with amplitude δw. The dispersions have been simulated in Lumerical using the ordinary and extraordinary refractive indices from Refs. [28] and [26].

For each system (a-e), we calculate the phase matching and the fidelity $\mathcal{F}$ of 20 randomly generated samples for every combination of the parameters in Table 1.

To aid in visualization, a randomly chosen subset of the calculated values of $\mathcal{F}$ is presented in Fig. 2. It is apparent that the fidelity of the simulated processes closely follows the model derived in the previous section, despite having different noise sources and being realized in vastly disparate physical systems. This shows that the model presented provides a general framework to analyze the effects of inhomogeneities on the phase-matching performance of a wide range of nonlinear systems.

In this Letter, a general framework for the description and understanding of the phase matching of nonlinear processes in the presence of momentum mismatch variations has been developed. In particular, we have shown that the shape of the phase-matching spectrum of a wide class of nonlinear systems is uniquely determined by the *noise-length product*σL and the noise profile $\delta\beta(z)$. This result shows that it is possible to study the effect of variations of $\Delta\beta$ independent of the specific physical properties of the nonlinear systems and of the sources of imperfections.

Using this framework, we investigated the effect that a noise profile $\delta\beta(z)$ with a $1/f$ noise spectrum has on the

Table 1. Fabrication Parameters Used for the Simulation of (a) Ti:LN Waveguides, (b) Channel Rb:KTP Waveguides, (c) LN Bulk Crystals, (D) PCFs, and (e) LNOI Waveguides[a]

(a)	$L = 5, 10, 40, 80$ mm
	$\delta w = 0.05, 0.1, 0.25, 0.5$ μm
(b)	$L = 5, 10, 15, 20, 25, 30$ mm
	$\delta w = 0.05, 0.1, 0.2, 0.3, 0.5$ μm
(c)	$L = 5, 10, 20, 40$ mm
	$\delta T = 0.1, 0.2, 0.5, 1.0, 2.0$°C
(d)	$L = 0.5, 1, 2, 3$ m
	$\delta d = 0.64, 6.41, 64.14, 641.44$ pm
(e)	$L = 0.1, 0.2, 0.5, 1.0, 2.0, 5.0$ mm
	$\delta w = 1, 2, 5, 10, 20, 50$ nm

[a]Details about the processes are provided in the main text.

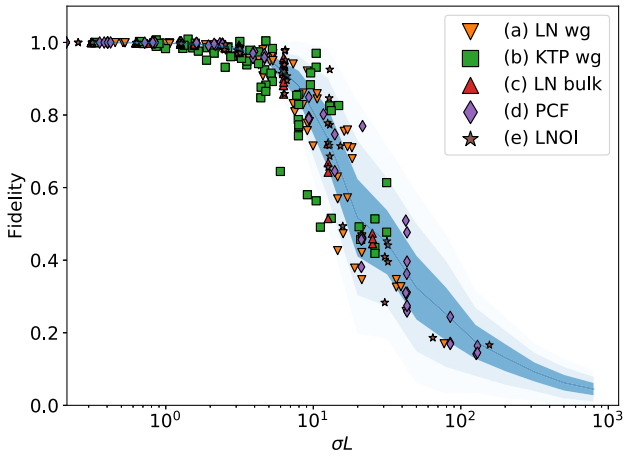

Fig. 2. Fidelity $\mathcal{F}$ simulated for different real systems in the presence of $1/f$ noise on a fabrication/operation parameter. The solid blue line represents the average fidelity as estimated by the general model, while the shaded areas correspond to 1, 2, and 3 standard deviations. Details about the processes are provided in the main text.

phase-matching spectrum, for different noise-length products. We introduced a process fidelity $\mathcal{F}$ to measure the ideality of a phase-matching spectrum and discovered that high fidelities ($\mathcal{F} > 0.8$) are found for systems with $\sigma L < 10$. This inequality provides a general design rule for realizing high-fidelity nonlinear processes.

We applied this design rule to analyze the case of fabrication errors in the PCF reported in Ref. [18]. The analysis was able to explain the reported phase-matching spectra and provide insight towards the requirements necessary to achieve a high-fidelity phase-matching spectrum.

Finally, we show that many different physical systems follow the trend predicted by the model. This shows that the presented framework provides a universal method to understand and compare the properties of a wide range of nonlinear processes.

Funding. Deutsche Forschungsgemeinschaft; European Commission–Horizon2020–UNIQORN (820474).

Acknowledgment. The authors thank Ganaël Roeland, Vahid Ansari, Jeremy Kelly-Massicotte, and Pete Mosley for helpful discussions.

REFERENCES

1. P. A. Franken, A. E. Hill, C. W. Peters, and G. Weinreich, Phys. Rev. Lett. **7**, 118 (1961).
2. D. J. Kane and R. Trebino, IEEE J. Quantum Electron. **29**, 571 (1993).
3. C. Iaconis and I. A. Walmsley, Opt. Lett. **23**, 792 (1998).
4. G. Harder, V. Ansari, B. Brecht, T. Dirmeier, C. Marquardt, and C. Silberhorn, Opt. Express **21**, 13975 (2013).
5. J. S. Pelc, L. Ma, C. R. Phillips, Q. Zhang, C. Langrock, O. Slattery, X. Tang, M. M. Fejer, G. N. Gol, O. Okunev, G. Chulkova, A. Lipatov, A. Semenov, K. Smirnov, B. Voronov, A. Dzardanov, C. Williams, and R. Sobolewski, Opt. Express **19**, 21445 (2011).
6. N. Maring, P. Farrera, K. Kutluer, M. Mazzera, G. Heinze, and H. de Riedmatten, Nature **551**, 485 (2017).
7. A. Eckstein, B. Brecht, and C. Silberhorn, Opt. Express **19**, 13770 (2011).
8. M. Santandrea, M. Stefszky, V. Ansari, and C. Silberhorn, New J. Phys. **21**, 033038 (2019).
9. E. J. Lim, S. Matsumoto, and M. M. Fejer, Appl. Phys. Lett. **57**, 2294 (1990).
10. S. Helmfrid and G. Arvidsson, J. Opt. Soc. Am. B **8**, 2326 (1991).
11. S. Helmfrid, G. Arvidsson, and J. Webjörn, J. Opt. Soc. Am. B **10**, 222 (1993).
12. J. S. Pelc, C. Langrock, Q. Zhang, and M. M. Fejer, Opt. Lett. **35**, 2804 (2010).
13. J. S. Pelc, C. R. Phillips, D. Chang, C. Langrock, and M. M. Fejer, Opt. Lett. **36**, 864 (2011).
14. C. R. Phillips, J. S. Pelc, and M. M. Fejer, J. Opt. Soc. Am. B **30**, 982 (2013).
15. R. Nouroozi, J. Lightwave Technol. **35**, 1693 (2017).
16. M. Karlsson, J. Opt. Soc. Am. B **15**, 2269 (1998).
17. M. Farahmand and M. de Sterke, Opt. Express **12**, 136 (2004).
18. R. J. A. Francis-Jones and P. J. Mosley, Opt. Express **24**, 24836 (2016).
19. T. Harlé, M. Barbier, M. Cordier, A. Orieux, E. Diamanti, I. Zaquine, and P. Delaye, "Influence of fibre homogeneity on Four Wave Mixing pair generation," in *Conference on Lasers and Electro-Optics (CLEO) Europe* (2017).
20. D. Chang, C. Langrock, Y.-W. Lin, C. R. Phillips, C. V. Bennett, and M. M. Fejer, Opt. Lett. **39**, 5106 (2014).
21. M. Santandrea, 2019, https://github.com/mattsantand/pynumericalphasematching.
22. F. R. Nash, G. D. Boyd, M. I. Sargent, and P. M. Bridenbaugh, J. Appl. Phys. **41**, 2564 (1970).
23. K. Saitoh and M. Koshiba, Opt. Express **13**, 267 (2005).
24. E. Strake, G. P. Bava, and I. Montrosset, J. Lightwave Technol. **6**, 1126 (1988).
25. P. T. Callahan, K. Shafak, P. R. Battle, T. D. Roberts, and F. X. Kärtner, Opt. Express **22**, 9749 (2014).
26. D. Jundt, Opt. Lett. **22**, 1553 (1997).
27. B. Desiatov, A. Shams-Ansari, M. Zhang, C. Wang, and M. Lončar, Optica **6**, 380 (2019).
28. G. J. Edwards and M. Lawrence, Opt. Quantum Electron. **16**, 373 (1984).